Proceedings of the 4th International Conference on Computing Innovation and Applied Physics
DOI: 10.54254/2753-8818/87/2025.20350

# *The Microscopic World: Design and Construction a Low-Cost, Portable Reflective Digital Holographic Microscope*

**Lezhe Wang[1,a,*]**

[1]*Shanghai World Foreign Language Academy, Shanghai, China*
*a. 3498708783@qq.com*
**corresponding author*

***Abstract:*** In daily life, scratches are often left on reflective surfaces, including rearview mirrors, makeup mirrors, and optical lenses, posting significant problems on image quality. Traditional 3D measurement methods usually use expensive and massive instruments, such as confocal microscopes or electron microscopes, which are not practical for high school research projects. Digital microscopy has the advantages of being non-contact, full-field, real-time, and high-precision, offering a solution. Therefore, this paper explores the use of digital holographic microscopy to measure the 3D surface of reflective surfaces. The study is based on a Michelson interferometer, reducing the system's size by using folded optical path and eliminating unnecessary converging lenses. Through simulation experiments, this research explores how various optical system parameters affect imaging quality and optimizes the clarity of the 3D reconstruction. Based on the conclusions from the simulations, hardware set-up of the system was selected, including a 635nm laser, collimation lenses, a beam splitter, mirrors, and a CMOS camera, keeping the total cost under 3000 yuan. In the experimental section, the system was built, and through adjustments in the reference beam angle and the distance between the object and the camera, clear interference fringes were successfully obtained. To further enhance the research, MATLAB was used to write an angular spectrum diffraction reconstruction algorithm. The experiments conducted on lenses and wafers produced their 3D profiles. This research demonstrates the potential of digital microscopy in both solving real-world problems and helping high school students explore the field of physics, promoting a deeper understanding of concepts like optical interference and diffraction.

***Keywords:*** Digital holographic microscopy, Interferometry, 3D imaging.

## 1. Introduction

Microscopy is applied in every aspect of life. For instance, scratched glasses are a major issue in life. Apart from worsening image qualities, they even increase the risk of bacterial growth, harming eye health. To address the problem, people typically use touch to roughly measure the size and the shape of the scratch. However, this method is highly imprecise and inconvenient. This led me to consider how we can precisely measure the fine scratches on mirror surfaces using microscopy technology.

© 2025 The Authors. This is an open access article distributed under the terms of the Creative Commons Attribution License 4.0 (https://creativecommons.org/licenses/by/4.0/).

DOI: 10.54254/2753-8818/87/2025.20350

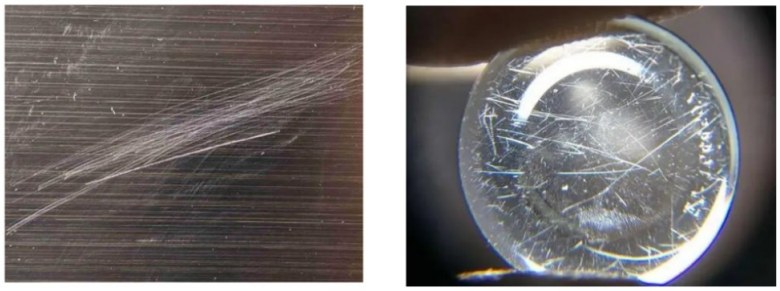

(a) (b)

Figure 1: (a) Scratched mirror (b) Scratched contact lens

Beyond daily life, precise microscopic measurement plays an even more significant role in industrial applications. With advances in manufacturing technology, there is a growing demand for ultra-precision processing in fields including national defense, modern communications, and medical devices. The precision, miniaturization, and flexibility required for mechanical manufacturing set higher standards for machining capabilities, with processing accuracy now reaching the range of 0.1 to 0.01 micrometer.

Among them, advanced ceramics or optical glass elements with reflective surfaces, require exceptionally high shape precision, surface quality, and minimal machining damage layers. Understanding the material removal patterns and the characteristics of the damage layer during ultra-precision machining is crucial for improving both stability and economic efficiency [1]. Microscopic instruments must be used during mechanical manufacturing to test surface parameters and specifications to ensure they meet quality standards. However, the high cost of existing surface measurement technologies has hindered the widespread adoption of ultra-precision machining at a lower cost. For instance, the digital holographic microscopes produced by the Swiss optical company Lyncee Tec can cost upwards of 1 million yuan. To further promote precision machining and measurement, it is essential to reduce the cost of precision testing technology while maintaining quality.

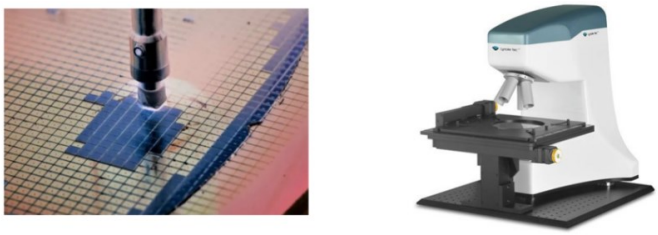

(a) (b)

Figure 2: (a) 3D imaging of chips (b) Digital holographic microscope from Lyncee Tec

Building on these issues, in this research, I selected the reflective holographic microscopy as the technology. I first studied the fundamental theories of digital holographic microscopy. The research is conducted through both the hardware system and software algorithms: In the hardware, I designed and built the optical system based on the Michaelson interferometer, selecting optimal parameters and reducing the size by using folded optical path and eliminating unnecessary converging lenses. To advance the study, I developed an angular spectrum reconstruction algorithm using MATLAB. During the experiment, I measured the 3D surfaces of both lenses and silicon wafers. This research not only demonstrated the capability of digital holographic microscopy to solve practical problems but also combines the advanced scientific concepts with everyday scenarios.

DOI: 10.54254/2753-8818/87/2025.20350

## 2. Digital holographic microscopy (DHM) theory

### 2.1. Digital holographic recording

The first step of DHM is wavefront recording: The interference pattern of the object wave and the reference wave is discretely sampled by a CCD or CMOS camera into a 2D matrix, which is then stored on a computer. This matrix is called the digital hologram.

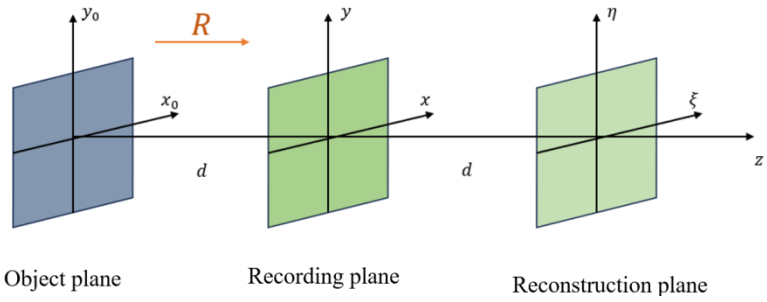


Figure 3: Digital holographic recording and reconstruction

As shown, plane $(x_0, y_0)$ is the object plane, $(x, y)$ is the recording plane of the CCD or CMOS camera, and plane $(\xi, \eta)$ is the reconstruction plane. The object wave propagating to the recording plane is expressed as:

$$O(x,y) = o(x,y)exp\,[-j\varphi(x,y)] \tag{1}$$

The reference wave propagating to the recoding plane is:

$$R(x,y) = r(x,y)exp\,[-j\varphi(x,y)] \tag{2}$$

The intensity distribution of the hologram formed by the interference of the object wave and the reference wave on the recording wave is calculated as:

$$\begin{aligned} I(x,y) &= |O(x,y) + R(x,y)|^2 \\ &= |O(x,y)|^2 + |R(x,y)|^2 + O(x,y)R^*(x,y) + O^*(x,y)R(x,y) \end{aligned} \tag{3}$$

Here, $|O(x,y)|^2$ is the intensity distribution of the object wave, $|R(x,y)|^2$ is the intensity distribution of the reference wave, which do not contain phase information and are called zero-order terms or DC components. The third term contains the complex amplitude distribution of the object wave $O(x,y)$, the numerical reconstruction of which results in the real image of the object wave, known as the positive first-order term. The fourth term is the conjugate of the original object wave's complex amplitude distribution $O^*(x,y)$, and reconstructing this term results in a virtual image, known as the negative first-order term or conjugate image, which acts as a noise component [2].

### 2.2. Digital holographic reconstruction

Diffraction is a common characteristic of wave propagation. Similar to traditional holography, digital holography uses the principle of diffraction to reconstruct the image. As shown in the Figure 3, in digital diffraction holographic reconstruction, the reconstruction wave is simulated by the computer and multiplied with the stored hologram at the recording plane. The resulting wave is propagated to the reconstruction plane $(\xi, \eta)$.

Let the simulated reconstruction wave at the recording plane be C(x, y). Then, the field distribution $T(x,y)$ after multiplying the hologram image $I(x,y)$ with the reconstruction wave can be expressed as:

DOI: 10.54254/2753-8818/87/2025.20350

$$T(x,y) = C(x,y)I(x,y) = C(x,y)|O(x,y) + R(x,y)|^2 = C(x,y)|O(x,y)|^2 + C(x,y)|R(x,y)|^2 + C(x,y)O(x,y)R^*(x,y) + C(x,y)O^*(x,y)R(x,y) \quad (4)$$

Here, the first and second terms contain only the intensity and phase information of the object and reference waves and not the phase information of the object wave, so they are referred to as zero-order diffraction images. The third term contains information about the object wave $O(x,y)$, and when the reconstruction wave matches the reference wave, an undistorted virtual image of the object can be reconstructed at the original object plane. This is the positive first-order diffraction image. The fourth term contains the conjugate wave information of the object wave $O^*(x,y)$, and when the reconstruction wave is conjugated with the reference wave, an undistorted real image can be obtained at a distance d in front of the hologram recording plane. This is called the negative first-order diffraction image. When reconstructing the original object wave, the zero-order image can be treated as noise, as it does not contain phase information. Both the positive first-order and negative first-order terms contain object wave information, but since they are conjugates of each other, they interfere with one another, so only one of the terms can be selected for reconstruction[3].

Depending on the optical path design, digital holographic systems can be classified into on-axis and off-axis configurations. In on-axis configurations, the object and reference waves are aligned at an angle of 0°, causing the zero-order diffraction image and the ±1st order diffraction images to overlap. To separate the three spectral components, hardware phase-shifting methods or software phase iteration algorithms are required to reconstruct the object wave: Phase-shifting methods demand extremely precise hardware, while iterative algorithms are time-consuming [4]. Considering cost and feasibility, my system employs an off-axis configuration, where the object and reference waves have a small angle between them. The off-axis hologram contains dense carrier fringes, with the zero-order diffraction image located at the center of the spectrum, and the ±1st order diffraction images positioned in opposite quadrants, allowing for direct selection of one first-order term for reconstruction.

The diffraction propagation of light wave can be simulated using multiple methods, such as the Fresnel transform, convolution method, and angular spectrum method. Among these, the Fresnel transform and convolution methods are not suitable for short-distance diffraction propagation due to limitations in discrete sampling. In contrast, the angular spectrum method is based on the theory of plane waves and strictly follows the scalar diffraction Helmholtz equation. It provides an accurate representation of diffraction in the frequency domain, without the limitations imposed by short diffraction distances. The transmission function of the angular spectrum propagation can be expressed as:

$$U(f_\xi, f_\eta) = T(f_x, f_y)H(f_x, f_y) = C(f_x, f_y)I(f_x, f_y)H(f_x, f_y) \quad (5)$$

, where $H(f_x, f_y)$ is the transfer function of wave propagation in free space [5]:

$$H(f_x, f_y) = exp\left[j\frac{2\pi}{\lambda}z_i\sqrt{1 - (\lambda f_x)^2 - (\lambda f_y)^2}\right]$$

$$\Delta\xi = \frac{1}{M\Delta x}, \Delta\eta = \frac{1}{N\Delta y} \quad (6)$$

The complex amplitude information of the object wave can be obtained by applying the inverse 2D discrete Fourier transform (IDFT) to $U(f_\xi, f_\eta)$:

$$\begin{aligned} G(x_0, y_0) &= IDFT\{C(f_x, f_y)I(f_x, f_y)H(f_x, f_y)\} \\ &= IDFT\{DFT[C(x,y)I(x,y)]H(f_x, f_y)\} \end{aligned} \quad (7)$$

DOI: 10.54254/2753-8818/87/2025.20350

It can be concluded that, in the angular spectrum method, the hologram first has to be transformed to the frequency domain via 2D discrete Fourier transform (DFT), and then be transformed back to the space domain via IDFT. Therefore, equal pixel size at both the recording plane and reconstruction plane is more efficient and straightforward in practical calculation.

After obtaining the complex amplitude information, the intensity and phase of the object wave can be recovered using the following formulas:

$$I_0(x_0, y_0) = \left|G(x_0, y_0)\right|^2$$
$$\varphi_0(x_0, y_0) = arctan\left\{\frac{Im\left[G(x_0,y_0)\right]}{Re\left[G(x_0,y_0)\right]}\right\} \tag{8}$$

However, the range of the arctan function is $\left[-\frac{\pi}{2}, \frac{\pi}{2}\right]$, which is reconstructed to $[-\pi, \pi]$ using quadrant determination. This means that the recovered longitudinal depth is less than the wavelength of the recorded light wave, and the phase is in a wrapped state. The phase unwrapping process will be covered in the following section.

## 2.3. Phase Unwrapping

Phase unwrapping is the process of recovering the true phase distribution from wrapped phase data using an algorithm. According to the Shannon sampling theorem, the interpolation of adjacent phases within the 2D phase array must lie in the range of $(-\pi, \pi]$ for discrete sampling. Thus, phase unwrapping involves adding or subtracting integer multiples of $2\pi$ to ensure the continuity of adjacent phase relationships. The relationship between the true phase value $\varphi$ and the wrapped phase value $\phi$ is:

$$\phi(x, y) = W[\varphi(x, y)] = mod(\varphi(x, y), 2\pi) \tag{9}$$

,where WWW is the wrapping operator, which limits the wrapped phase $\phi$ to the range $(-\pi, \pi]$. Global or local phase unwrapping algorithms can be used to recover the unwrapped phase information [6].

## 2.4. Principle of reflective digital holographic microscopy

For a reflective holographic microscope. The light wave carries the phase information of the object when reflecting off the object's surface. Thus, after obtaining the 3D phase information of the object, its corresponding height information can be reconstructed. Since this study only investigates reflective objects, the influence of different refractive indices on the optical path is not taken into consideration in calculation. Therefore, the height is directly calculated from the phase difference $\Delta\varphi$. Due to the reflection of light, the optical path difference $\Delta l$ is twice the height $h$, such that $\Delta l = 2h$.

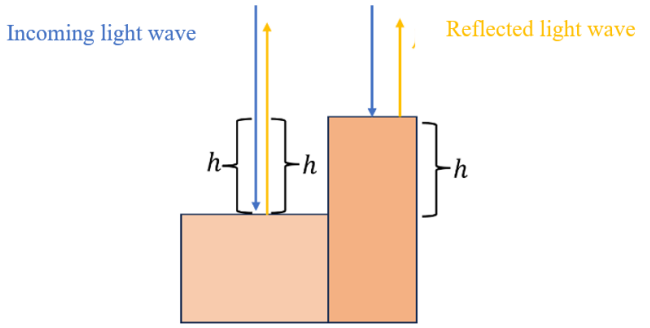


Figure 4: Illustration of imaging of a reflective surface

DOI: 10.54254/2753-8818/87/2025.20350

The optical path difference is the product of the wave number and the phase difference $\Delta\varphi$:

$$\Delta l = \frac{\lambda}{2\pi} \cdot \Delta\varphi$$

Thus, the height $h$ can be calculated as:

$$2h = \frac{\lambda}{2\pi} \cdot \Delta\varphi$$

$$h = \frac{\lambda \cdot \Delta\varphi}{4\pi} \tag{10}$$

## 3. Design and construction of the microscopic system

### 3.1. Optical path design

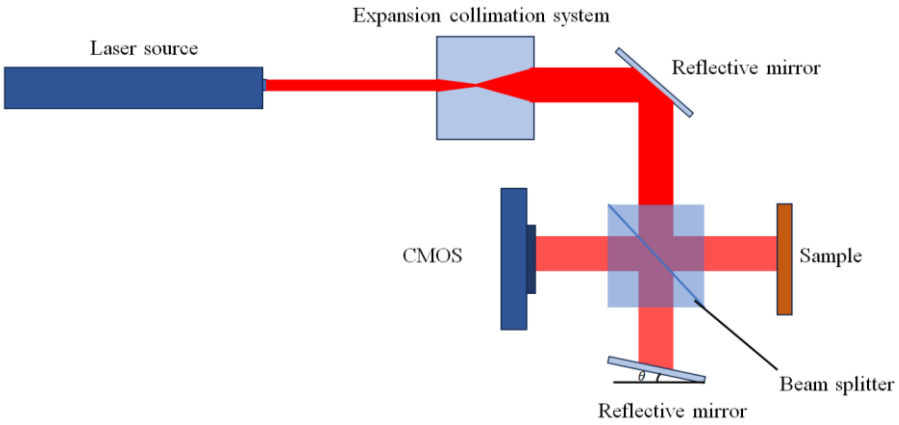


Figure 5: Reflective digital holographic optical path

The optical path design is shown in the Figure 5. The monochromatic laser is emitted from the laser source and magnified by the expansion collimation system of lenses. The ideal magnification of the system is between 3x and 4x. The laser is then reflected by a mirror and directed to a beam splitter prism, where half of the light is transmitted to another mirror and half is reflected to the sample plane. The transmitted light is the reference wave since it does not carry the 3D information of the sample; the reflected light, from which the 3D information of the sample can be reconstructed, is the object wave. Since there is a small angle θ between the mirror and the horizontal, the object and reference waves also form a small angle θ, generally between 1° and 3°. Therefore, this system is classified as an **off-axis optical path**. The reference wave is reflected and directed to the beam splitter again, with half of it being reflected to the CMOS camera; the object wave carries 3D information after reflection, with half of it being transmitted to the CMOS camera at the beam splitter. The interference fringes formed by the two light waves are recorded by the camera's sensor and stored digitally.

### 3.2. Selection of system instruments

Based on the optical path design, the reflective holographic microscope consists of the following instruments.

1. **Optical platform**: The M6 optical platform with the dimension of 30*30*50 $cm^3$ is chosen as the base of the holographic system. Numerous optical posts of 10 cm and post holders of 5 cm and 10 cm are used to fix the positions and directions of the instruments. The expansion collimation system and beam splitter have specified requirements of distances between instruments, so clamping forks are used to position them at the positions other than the slots of the platform.

DOI: 10.54254/2753-8818/87/2025.20350

Meanwhile, since the interference mirror requires fine adjustments in the angle, it is supported by a 2D mirror mount. The laser and lenses are fixed in positions by the mounts with corresponding diameters.

2. **Laser source**: Common light sources for digital holographic systems include lasers and low-coherence light sources. Low-coherence sources have a broad spectrum and short coherence length, making optical path adjustment difficult. Therefore, I chose a laser source due to the following advantages: (1) good monochromaticity and high coherence, (2) low divergence angle, and (3) concentrated energy. The specific model used is the GCI-07-635-5 from Daheng Imaging, with a wavelength of 635 ± 10 nm and a power of 5 mW.
3. **Beam expander and collimation System**: This system enlarges the collimated input beam into a larger-diameter collimated output beam. It consists of two lenses with different focal lengths, so the magnification is the ratio of the focal lengths of the two lenses. I used two plano-convex lenses to construct a 3x beam expander, with the lens diameters and focal lengths as follows: (1) diameter 10 mm, focal length 10 mm, and (2) diameter 25.4 mm, focal length 30 mm.
4. **Beam splitter prism**: A beam splitter prism was used to shorten the optical path distance and reduce the system's overall size. The dimensions of the prism are 25 x 25 x 25 mm, and I custom-designed an acrylic plate to hold the prism in place.
5. **Mirrors**: The system uses two mirrors: one for shortening the optical path and one for generating interference. For the optical path shortening, I used a 30 x 30 x 30 mm non-coated right-angled prism, which is cost-effective. For interference, I used a 25.4 mm silver-coated mirror produced by Finner, which offers superior reflectivity but is more expensive.
6. **Z-axis manual lifting stage**: The sample is positioned on the lifting stage, which allows for precise height adjustments by turning a knob, ensuring that the distances between the object and reference waves are equal. The stage dimensions are 40 x 40 mm, with a Z-axis travel range of ±5 mm, a load capacity of 2 kg, and a thickness of 35-45 mm.
7. **CMOS camera**: The camera converts the optical signal into an electrical signal for imaging. Since the system does not require color information, I selected a black-and-white CMOS camera to reduce costs. The specific model is the MV-SUM133GC/M-T-B, with a pixel size of 4 μm, a resolution of 1280 x 1024, a frame rate of 245 FPS, and support for continuous triggering.




Figure 6: Laser source GCI-07-635-5 and CMOS MV-SUM133GC/M-T-B

### 3.3. Construction and adjustment of the optical path

The construction of the system followed the optical path design:

First, the instruments are fixed to their corresponding mounts and positioned to the specific slots of the platform. The approximate directions are altered by rotating the optical posts.

When building the expansion collimation system, I measured a separation of 4 cm using a ruler, and then positioned the two lenses on the correct focal points. Due to the special requirement of the separation, the poles mounts cannot be fixed on the slots of the platform, so I used clamping forks and screws to adjust the position.

Since the right-angled prism cannot be fixed on the screw at the top of the optical post, I tried using a cut cupboard, which acts as a mount, to stabilize the prism. However, it easily leads to shaking

DOI: 10.54254/2753-8818/87/2025.20350

and deformation. Alternatively, I designed acrylic boards with corresponding dimensions and screw holes to hold the prism in place.

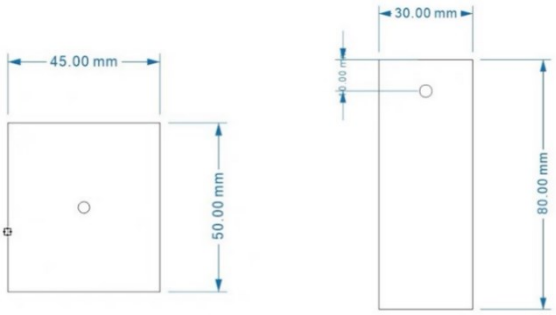


Figure 6: Acrylic boards design

The interference optical path required precise adjustments of the laser angle, camera height, and object distance. I custom-designed an acrylic plate to hold the beam splitter prism and camera at the correct positions and distances. After that, I secured the silver-coated mirror on the 2D mirror mount and locked it in place with screws. The position of the mirror was adjusted using the fine-tuning knobs on the 2D mount.

Once the system was assembled, I adjusted the optical path to ensure proper interference. Initially, I did not take safety precautions, and though the 5 mW laser was not directly harmful to the eyes, extended exposure caused discomfort and afterimages. I quickly purchased laser safety goggles (590-690 nm) and continued adjusting.

For the optical path adjustment, it should be ensured that the laser, lenses, prisms, and mirrors were aligned at the same height and had correct directions. The expansion collimation system was adjusted by placing the 10 mm focal length lens in front of the laser and using white paper to check for a uniform circular light spot. After placing the 30 mm focal length lens at a distance of 4 cm from the first lens, I made minor adjustments until the collimation was achieved.

The most challenging part was aligning the interference optics. I positioned the camera above the beam splitter prism and connected it to a computer to monitor real-time imaging. By adjusting the 2D mirror holder and the Z-axis manual stage, I corrected the angles and distances of the object and reference waves until the two light spots overlapped on the camera's image, indicating successful interference.

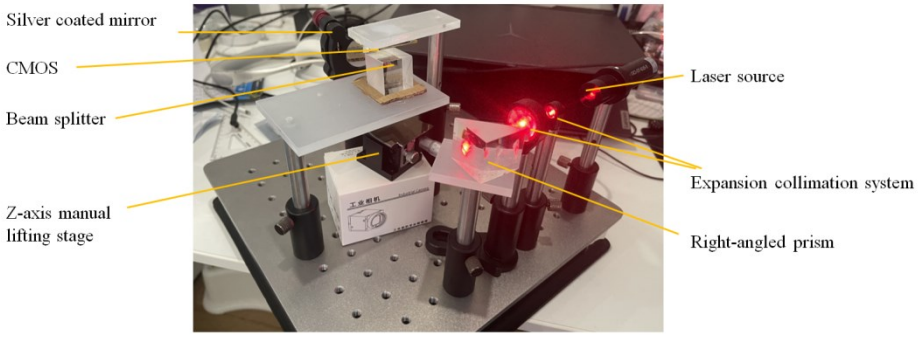


Figure 7: Adjusted digital holographic microscope system

DOI: 10.54254/2753-8818/87/2025.20350

# 4. Experiment and data processing

## 4.1. Data processing based on MATLAB

The data processing algorithm was implemented using MATLAB to handle holographic measurements. Based on equations from earlier sections, the overall processing flow is shown in the diagram below:

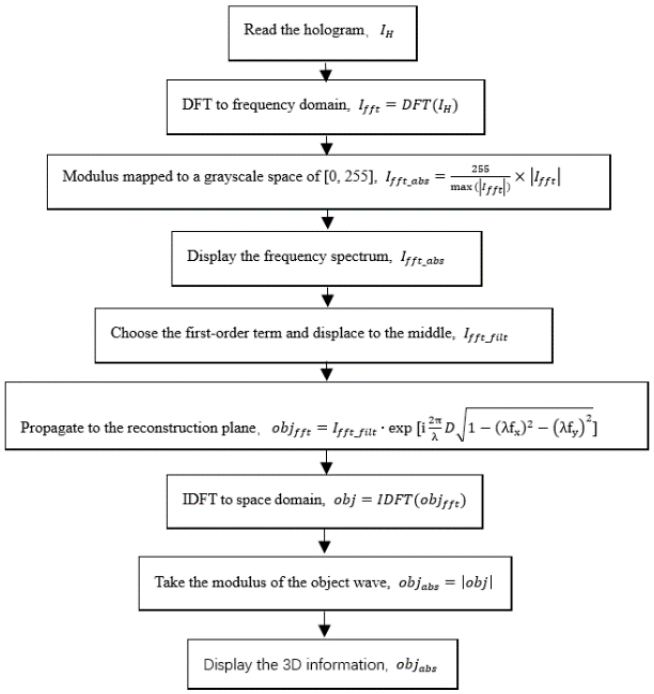


Figure 8: Data processing flowchart

## 4.2. Data processing of mirror

While assembling and calibrating the optical system, I used a fully reflective mirror to adjust the optical path. The mirror was placed on the Z-axis manual stage, and by changing the height of the stage, the distance between the object and the CMOS camera was varied. As the distance changed, the sharpness of the zero-order and conjugate images in the frequency spectrum varied. By continually adjusting the mirror's height and observing the frequency spectrum, I determined the height where the sharpest zero-order and conjugate images were obtained and used this position for calibration. Since even slight changes in the mirror's angle could greatly affect the position of the conjugate image, fine adjustments were made to the mirror's angle within the range of approximately 1° to 3°, ultimately obtaining a sharp and well-separated frequency spectrum. The experimental results are shown in the Figure 9.

DOI: 10.54254/2753-8818/87/2025.20350

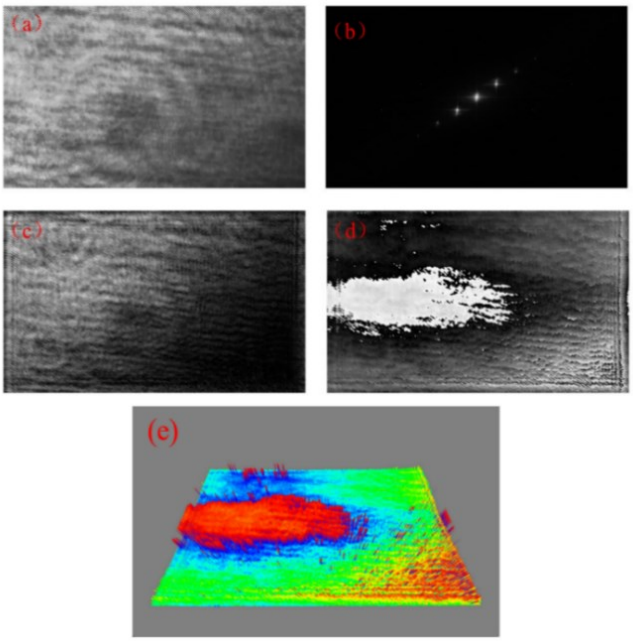


Figure 9: Results of mirror measurement (a) hologram (b) frequency spectrum (c) Intensity diagram (d) phase diagram (e)3D information By collecting holograms using the off-axis reflective digital holographic system, it is clear that the system can accurately detect surface defects and manufacturing errors on reflective mirrors.

### 4.3. Data processing of wafer

To further test the system's application in manufacturing industries, I purchased an 8-inch wafer from SMIC on Alibaba for measurement. A wafer is a silicon disc used for fabricating semiconductor circuits, composed of silicon. High-purity polycrystalline silicon is melted, and a silicon seed crystal is dipped in, such that a cylindrical single-crystal silicon ingot is formed. After grinding, polishing, and slicing, the silicon ingot is processed into silicon wafers. In China, 8-inch and 12-inch wafers are commonly produced.

Below are the measurement results:

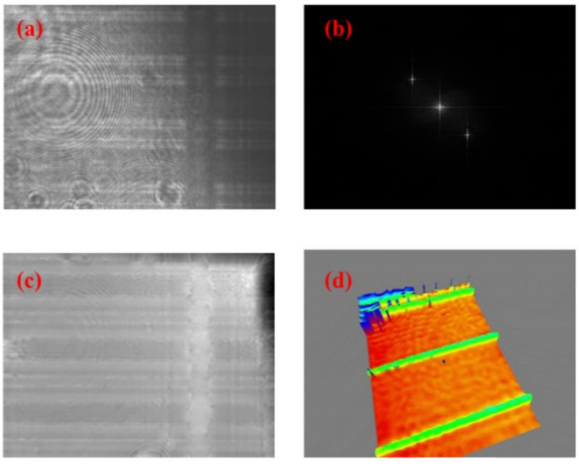


Figure 10: Results of wafer measurement (a) hologram (b) frequency spectrum (c) phase diagram (d)3D information

DOI: 10.54254/2753-8818/87/2025.20350

## 5. Conclusion

This paper explores the issue of mirror scratches in everyday life and investigates the measurement of 3D morphology of microscopic surfaces. First, a holographic microscopic system based on the Michelson interferometer optical path was developed. By folding the optical path and removing unnecessary converging lenses, the system was made more compact and efficient. Next, hardware components were carefully selected, including a 635 nm laser, beam expander collimation lenses, beam splitter prism, mirrors, and a CMOS camera, keeping the total cost below 3000 yuan.

In the experimental section, after setting up the system, I adjusted the off-axis angle of the reference wave and the distance between the object and the camera to ensure that the waves successfully interfered and produced clear interference fringes. To further enhance the research, an angular spectrum diffraction reconstruction algorithm was written using MATLAB. During experimental validation, both lenses and wafers were tested, and their 3D morphology was successfully obtained.

This study demonstrates the potential for reflective digital holographic technology to be applied in precision machining and educational fields, helping to reduce manufacturing and teaching costs and benefiting a wider audience. Overall, this research has given me a comprehensive understanding of the research process in the field of physics and has shown the potential for digital holography to solve real-world problems.

## References

[1] *Li, C., Tian, Y., & Yan, S. (2020). Laser scanning confocal microscopy technology and its applications. Experimental Science and Technology, (04), 33-38.*

[2] *Samanta, K., Tiwari, A., PT, S., & Joseph, J. (2024). Improving resolution in two orthogonal orientations from a single-shot digital holographic microscopy. Results in Optics, 14, 100586. https://doi.org/10.1016/j.rio.2023.100586*

[3] *Kim, M. K. (2010). Principles and techniques of digital holographic microscopy. Journal of Photonics for Energy, 018005. https://doi.org/10.1117/6.0000006*

[4] *Guo, R., Yao, B., Gao, P., Min, J., Zhou, M., Han, J., Yu, X., Yu, X., Lei, M., Yan, S., Yang, Y., Dan, D., & Ye, T. (2013). Off-axis digital holographic microscopy with LED illumination based on polarization filtering. Applied Optics, 52(34), 8233. https://doi.org/10.1364/ao.52.008233*

[5] *De Nicola, S., Finizio, A., Pierattini, G., Ferraro, P., & Alfieri, D. (2005). Angular spectrum method with correction of anamorphism for numerical reconstruction of digital holograms on tilted planes. Optics Express, 13(24), 9935. https://doi.org/10.1364/opex.13.009935*

[6] *Yan, L., Wang, Q., Huang, L., Chen, B., & Lin, Y. (2021). Phase unwrapping of digital holographic microscopy using adaptive region segmentation and phase derivative calibration with respect to fringe density. Optics and Lasers in Engineering, 148, 106780. https://doi.org/10.1016/j.optlaseng.2021.106780*